Title. Curing kinetics and effects of fibre surface treatment and curing parameters on the interfacial and tensile properties of hemp/epoxy composites

M.S.Islam[1][*], K.L.Pickering[1] and N.J.Foreman[2]

[1]*Department of Engineering, The University of Waikato, Private Bag 3105, Hamilton, New Zealand*

[2]*Hemptech, PO Box 46033, Herne Bay, Auckland, New Zealand*

Abstract

The curing kinetics of neat epoxy (NE) and hemp fibre/epoxy composites was studied and assessed using two dynamic models (the Kissinger and Flynn-Waal-Ozawa Models) and an isothermal model (the Autocatalytic Model) which was generally supported by the experimental data obtained from dynamic and isothermal differential scanning calorimetry (DSC) scans. The activation energies for the curing of composites exhibited lower values compared to curing of NE which is believed to be due to higher nucleophilic activity of the amine groups of the curing agent in the presence of fibres. The highest tensile strength, σ was obtained with composites produced with an epoxy to curing agent ratio of 1:1 and the highest Young's modulus, E was obtained with an epoxy to curing agent ratio of 1:1.2. Alkali treated hemp fibre/epoxy (ATFE) composites were found to have higher σ and E values compared to

*To whom correspondence should be addressed (Current address: CSIRO Materials Science and Engineering – Geelong, Belmont, Victoria 3216, Australia, Phone: +61352464022, Cell: +61413345047 Fax: +61352464057, E-mail: Saiful.Islam@csiro.au).

those for untreated hemp fibre/epoxy (UTFE) composites which was consistent

with the trend for interfacial shear strength (IFSS) values. Composites σ and E were found to

be higher for a processing temperature of 70°C than for 25°C for both UTFE and ATFE

composites, but were found to decrease as the curing temperature was increased further to

120°C.

Keywords: Hemp Fibre, Curing Kinetics, Interfacial Shear Strength, Dynamic and Isothermal

Models.

1. Introduction

Diglycidyl ether of bisphenol A (DGEBA) is the most common epoxy resin and is used

extensively in industry due to its fluidity and ease with which it can be processed [1]. It

possesses many desirable properties (e.g. high tensile strength, σ and Young's modulus, E,

excellent chemical and solvent resistance, good creep resistance and excellent fatigue

properties) which make it an ideal candidate as matrix for fibre reinforced composites [2]. The

physical properties of epoxy resins depend on the extent of cure, which depends on the curing

conditions, time and temperature of cure. Therefore, knowledge of curing kinetics for epoxy

resin is necessary to control curing in order to control physical properties.

Although epoxy resins can be cured with different curing agents, most studies performed to

date have been with amine curing agents [3-5]. These are highly reactive, low molecular

weight curing agents that result in tightly cross-linked networks [1]. A change in the structure

of the epoxy network on addition of other polymers might influence the reaction kinetics. The

addition of natural cellulose fibres to epoxy resins is thus expected to alter the curing kinetics.

While the curing kinetics of various neat epoxy resins and epoxy resins with other fillers has

been extensively studied mostly by using differential scanning calorimetry [6-9], the curing

kinetics of epoxy resins with natural fibres has not yet been studied.

The dynamic kinetic models proposed by Kissinger [10,11] and Flynn-Wall-Ozawa [12,13] are based on multiple-heating-rates. According to Kissinger [10], the activation energy can be calculated using the following relation:

$$\frac{d[\ln(q/T_m^2)]}{d(1/T_m)} = -\frac{E_a}{R} \tag{1}$$

where T_m is the exothermic peak temperature, q is the constant heating rate, E_a is the activation energy and R is the universal gas constant (8.314 J mol^{-1} K^{-1}). Therefore, a plot of $\ln(q/T_m^2)$ versus $1/T_m$ gives the activation energy without a specific assumption of the conversion dependent function.

The kinetic model developed by Flynn-Wall-Ozawa [12,13] calculates the activation energy as follows:

$$\log q = \log[\frac{AE_a}{g(\alpha)R}] - 2.315 - \frac{0.4567E_a}{RT_m} \tag{2}$$

where, $g(\alpha)$ is a kinetic model function that depends on the conversion and A is the pre-exponential factor. Using the above equation, the activation energy, E_a, can be calculated from a plot of $\log q$ versus $1/T_m$.

The isothermal Autocatalytic Model developed by Kamal [14] is a phenomenological approach. It assumes that at least one of the reaction products is involved in the propagating reaction, and thus is characterised by an accelerating isothermal conversion rate. The kinetics of autocatalysed reactions is described by the following equation [14]:

$$\frac{d\alpha}{dt} = k'\alpha^m (1-\alpha)^n \tag{3}$$

where m and n are the reaction orders and k' is the specific reaction rate constant. According to this model, the rate is zero or very small initially and attains a maximum value at some intermediate degree of conversion, typically between 20–40% conversion [15]. The initial rate of autocatalytic reactions may not necessarily be zero, as there is a possibility that reactants can be converted into products via alternative paths, only one of which is autocatalytic. To take these autocatalytic characteristics into account, a generalized expression can be used as follows:

$$\frac{d\alpha}{dt} = (k_1 + k_2\alpha^m)(1-\alpha)^n \tag{4}$$

where k_1 and k_2 are the reaction rate constants. Such a model has also been successfully applied to autocatalytic polymerization reactions [14,16]. In this case, the influence of the reaction products on the conversion rate is given by the term $k_2\alpha^m$.

The mechanical properties of fibre reinforced polymer composites are largely influenced by the interface. Several test methods (e.g. single fibre pull-out, fragmentation, microindentation, and push out) have been developed to characterise the interface and improve understanding of the adhesion between fibre and matrix resin [17,18]. Of these methods, the single-fibre pull-out test is the most commonly used method because of its ease of application and versatility [19]. The debonding force and embedded length are monitored during the pull-out process and the maximum pull-out force is converted to an apparent interfacial shear strength (IFSS) according to the following Kelly/Tyson Equation [20]:

$$\tau = \frac{F_{max}}{2\pi r l} \tag{5}$$

where F_{max} is the maximum debonding force, r is the radius and l is the embedded length of the fibre. Since the matrix is in compression during this test, the strength of the matrix is not a significant factor, thus allowing brittle matrices such as epoxy resins to be used [21]. There is

ample literature available with synthetic fibre/polymer matrix systems and assessment of their IFSS by single fibre pull-out tests [22-24]. However, very limited work has been reported regarding measurement of IFSS for natural fibres, especially by this technique [25,26].

The use of cellulose fibres as polymer reinforcement has increased over the last few years due to their low cost, low density, good specific mechanical properties, sustainability and biodegradability when compared to glass and aramid fibres [27,28]. Thermoset polymeric materials are attractive as matrix materials for natural fibre reinforced composite production as they generally have reactive functional groups that make them compatible with hydrophilic fibre surfaces [29]. Epoxy resins can form covalent cross-links with natural fibre via hydroxyl groups and therefore, they have potential for the development of high added value natural fibre composites to be used in the automotive industry [30].

To increase long-term stability of natural fibre composites and to improve interfacial bonding, researchers have attempted using various surface treatments of which alkali treatment with alkali has been found to be the most feasible [31]. Na_2SO_3 is also commonly used with alkali during the production of pulp to soften the lignin in the pulp and paper industry. Bledzki, Fink and Specht [32] used hemp fibres and investigated the influence of mercerization treatment on the properties of unidirectional epoxy resin model composites and reported an increase of flexural strength up to about 50% and flexural modulus up to about 100%. Wang and Postle [33] applied a weak (1.9 wt%) NaOH solution containing sodium sulphite (0.2 wt% Na_2SO_3) and sodium carbonate (0.2 wt% Na_2CO_3) to remove non-cellulosic materials from Australian hemp fibres and observed reduction of lignin and pectin. Gassan and Bledzki [34] obtained increases in yarn TS and YM of about 120% and 150% respectively, for tossa jute fibre using a 25 wt% NaOH solution. Alkali treatment of fibres has also been seen to increase the

crystallinity [35], molecular alignment of cellulose, surface roughness of the fibre [25] and to remove noncellulosic materials.

In this work, curing kinetics of NE and composites were studied using two dynamic kinetic models (the Kissinger and Flynn-Wall-Ozawa models) and an isothermal model (the Autocatalytic Model). Both dynamic and isothermal models were used to investigate the activation energies of an epoxy system containing DGEBA and an amine curing agent. The effect of addition of 40 wt% untreated hemp fibre on the activation energies of the same epoxy resin system was also studied. The aim of this study was also to investigate the effect of alkali fibre treatment of hemp fibre and different epoxy to curing agent ratios on the IFSS of hemp/epoxy composites obtained by single fibre pull-out tests. The influence of alkalisation with Na_2SO_3 as well as different epoxy to curing agent ratios and curing temperatures on the tensile properties of aligned hemp fibre/epoxy composites was also explored.

2 Experimental

2.1 Materials

Retted bast hemp fibre was supplied by Hemcore, UK. Epoxy resin (R180) with an amine curing agent (H180) was obtained from Fibreglass International, Australia. Analytical grade Na_2SO_3 and 98% NaOH pellets were used for the treatment of the fibres.

2.2 Methods

2.2.1 Treatment of the fibres with alkali

Pieces of the woody core present in the retted hemp bast fibre were manually removed. After weighing, fibres were placed into stainless steel canisters of 1L capacity. Pre-weighed NaOH and Na_2SO_3 solutions were then poured into the canisters such that the fibre to Na_2SO_3 solution to NaOH solution ratio was 1:2:10 by weight. The canisters were then placed into a

small lab-scale pulp digester at 120°C for 60 minutes for alkali treatment of the fibres. Fibres were washed in a pulp and paper fibre washer for about 45 minutes after the alkali treatment to remove chemical residues until a fibre pH of about 7 was obtained. Fibres were then dried in an oven for 48 hours at 70°C.

2.2.2 Curing kinetics of NE and UTFE composites using DSC

Thermal analysis (dynamic and isothermal) of the curing reaction of NE and 40 wt% UTFE composite samples was carried out using a DSC 2920 differential scanning calorimeter. An epoxy resin to curing agent ratio of 1:1 was used for both NE and 40 wt% UTFE composite samples. The weight of each specimen was set at approximately 10 mg. For 40 wt% UTFE composite samples, untreated fibres of 1 mm in length were placed in an aluminum pan. The uncured epoxy resin pre-mixed with curing agent was then poured on the fibres, ensuring wetting of the fibres with the mixture. The fibre-resin samples were then enclosed putting lids on the aluminum pans and scanned immediately, maintaining a static air flow of 50 mL/min. Dynamic scans of NE and 40 wt% UTFE composite samples were carried out at five different heating rates (2.5, 5, 10, 15, and 20°C/min) from room temperature to 250°C. For isothermal analysis, initially a steady isothermal baseline was established for each of the four selected cure temperatures (25, 50, 70, and 120°C) using two empty aluminum sample pans. Isothermal scans of NE and 40 wt% UTFE composite samples were then carried out such that the curing reactions were considered complete when the isothermal DSC thermograms levelled off to the baseline. Similarly, isothermal scans of NE and 40 wt% UTFE composite samples at three further epoxy to curing agent ratios of 1:0.6, 1:0.8, and 1:1.2 were carried out at 25°C.

2.2.3 IFSS measurement of hemp fibre/epoxy samples using single fibre pull-out testing

For the measurement of IFSS, single-fibre pull-out test specimens were prepared according to

the literature [36] using a silicone rubber block 12 mm long, 10 mm wide, and 3 mm deep. A 6 mm diameter circular hole was punched from the centre of the top face of the block through the depth of the material. Along the 12 mm length side of the block wall a slot was cut from the centre of the length to the edge of the circular hole to a depth of 2 mm as shown in Figure 1. Eight different embedded lengths from 0.25 mm to 2 mm at 0.25 mm intervals were produced by placing dried single fibres into the 2 mm slot with the required length extending into the block for four different epoxy resin to curing agent ratios (1:0.6, 1:0.8, 1:1 and 1:1.2). The embedded lengths were measured by placing the silicone rubber block under an electron microscope with a calibrated eyepiece at 50× magnification, while a calibrated eyepiece at 200× magnification was used to determine the average diameter of each embedded fibre. The hole at the centre of the block was filled with epoxy resin and cured at room temperature (20±2°C) for 24 hr using a vacuum bag and post cured at 50°C in an oven for 4 hr. Figure 2 shows a single fibre embedded in epoxy resin. The free end of the fibre that had been contained within the mould slot was glued to a cardboard using polyvinyl acetate (PVAc) glue to give a gauge length of 10 mm. Five specimens were prepared at each embedded length for both untreated fibre/epoxy (UTFE) and alkali treated fibre/epoxy (ATFE) samples and the average debonding force of the five specimens was measured using an Instron tensile tester at a crosshead speed of 0.5 mm/min.

2.2.4 Production of pre-form fibre mats

For the production of long fibre/epoxy composites, fibres were dried at 80°C for 24 hr to produce fibre mats using the following two methods:

(1) 60 g of dried fibres were aligned by hackling (by hand) to maintain a thickness of 3.5 mm, and (2) 60 g of dried fibres were aligned using a hand carding machine from Ashford Handicrafts Limited, Ashburton, New Zealand to maintain a thickness of 3.5 mm.

2.2.5 Production of composites

(a) Composites produced using different epoxy to curing agent ratios

Fibre mats were placed in a mould and epoxy resin was then poured onto the mats and allowed to soak into the fibres for 10 minutes. Four different epoxy resin to curing agent ratios (1:0.6, 1:0.8, 1:1, and 1:1.2) were used. A hand roller was used to remove the excess resin from the fibre mats resulting in 30 wt% and 40 wt% of fibres in the composites. The epoxy resin soaked fibre mats were placed in a vacuum bag and cured under vacuum for 24 hours at room temperature ($25^{o}C$) followed by post curing of the composite mats in an oven at $50^{o}C$ for four hours.

(b) Composites produced using different curing temperatures

Fibre mats were placed in an epoxy resin (epoxy to curing agent ratio of 1:1) bath for about 1 hr. The resin soaked mats were then fabricated into composites by placing in a pre-heated mould (the mould was heated using an oven) at three different curing temperatures and compressed at a pressure of 9.4 MPa. The duration of the pressure maintained (the pressure was maintained using pressure control valve of the compression mould) at each curing temperature was based on completion of the curing reaction as observed from thermal analysis results obtained from curing kinetics study (Table 1). Composites were produced at each of the three curing temperatures with 40 wt% fibre.

2.2.6 Composite tensile testing

The composite mats were cut into tensile test specimens using a computer numerical controlled (CNC) mill according to ASTM D638-03 standard test method for Tensile Properties of Plastics. The samples were then placed in a conditioning chamber at $23^{o}C \pm 3^{o}C$ and $50\% \pm 5\%$ relative humidity for 40 hr. The specimens were then tested using an Instron-4204 tensile testing machine fitted with a 5 kN load cell at a rate of 5 mm/min. An Instron

2630-112 extensometer was used to measure strain.

2.2.7 SEM Investigation

The morphology of the fracture surfaces of the tensile tested specimens was studied using a Hitachi S-4000 Field Emission SEM operated at 5 kV. Carbon tape was used to mount the samples on aluminum stubs. The samples were then sputter coated with platinum and palladium to make them conductive prior to SEM observation.

3. Results and discussion

3.1 Curing kinetics of NE and UTFE composites

3.1.1   Activation energies obtained using the dynamic Kissinger and Flynn-Wall-Ozawa Models (epoxy to curing agent ratio 1:1)

Activation energies were calculated using the Kissinger and Flynn-Wall-Ozawa Models and the peak temperature (T_m) and the total heat of reaction (ΔH_{tot}) obtained from DSC for both NE and composites for each heating rate. Figures 3 and 4 show the DSC exotherms obtained at different heating rates for NE and composites, respectively. From these figures it can be seen that the exotherm peak is found at increasingly higher temperatures as the heating rate increases. The total heat of reaction (ΔH_{tot}) values for the NE and composites were taken as the average of the heat of reaction (ΔH_0) values obtained at different heating rates as per other researchers [37,38]. To calculate the heat of reaction (ΔH_0) at each heating rate, the total area under each exotherm was determined. These results along with the peak temperatures of the exotherms are summarised in Table 2. It was observed that the ΔH_0 values did not vary much with the increase of heating rate for either NE or the composites. A similar lack of variation with NE was observed by Lopez . [39]. From the results (Table 2), it was also observed that the heat of reaction at the same heating rate and the total heat of reaction were lower for the

composite samples than for NE which might be due to the enhanced nucleophilic activity of the amine groups of the curing agent in presence of the fibre [40].

The exotherms (Figures 3 and 4) were analysed to obtain activation energies. Based on the Kissinger Model (Equation 1), the activation energies E_a were obtained from the plots of $\ln(q/T_m^2)$ versus $1/T_m$ for NE and composites (Figure 5). An approximately linear relationship was observed here, supporting the validity of the proposed model given in Equation 1. The activation energies E_a were calculated from the slopes, yielding values of 56.7 and 50.9 kJ/mol (Table 3) for NE and composites, respectively. The lower activation energy of the composites compared to that of NE indicates that fibre addition enhances the reaction rate, supporting the enhanced nucleophilic activity of amine groups in curing agent. The value for the activation energy of NE agreed reasonably well with the activation energies of similar epoxy/amine systems obtained by other researchers [41].

Based on the Flynn-Wall-Ozawa Model (Equation 2) activation energies were calculated from the slopes of the plots of $\log q$ versus $1/T_m$ for NE and composites [42] (Figure 6). An approximately linear relationship was observed, supporting the validity of the proposed model given in Equation 2. The activation energies thus obtained were 58.5 and 54.6 kJ/mol (Table 3) for NE and composites respectively. The lower activation energy for NE compared to that for composites is in agreement with the trend found for the Kissinger Model although the values are slightly higher than the activation energies obtained by the Kissinger Model. Other researchers have also reported that the activation energies of NE obtained from the Flynn-Wall-Ozawa Model were higher than those for the Kissinger Model [39,41].

3.1.2 Activation energies obtained using the Isothermal Autocatalytic Model

To calculate activation energies of NE and composites using the Autocatalytic Model (Equation 4), the kinetic parameters k_1 and k_2 of the model were used as per other researchers

[15]. To calculate these kinetic parameters, the time required for cure to occur, the heat of reaction obtained from an isothermal scan at time t (ΔH_t), and the final degree of cure (α_f)) collected from isothermal DSC scans which were carried out at four different curing temperatures (Table 4) were used.

At the start of the cure reaction ($t = 0$ and $\alpha = 0$), Equation 4 can be simplified to:

$$\left[\frac{d\alpha}{dt} \right]_{t=0} = k_1 \qquad (6)$$

Thus, the kinetic parameter, k_1 for both NE and composites was determined directly from isothermal reaction rate curves by extrapolating to zero time and is given in Table 5. For determination of the kinetic parameter, k_2 and other kinetic parameters m and n of the model, different calculation approaches, have been used by other researchers [15,43]. However, the graphical–analytical method used by Kenny [44] was applied in the present study to calculate the kinetic parameters k_2, m and n (Table 5) due to its ease of use. The detailed calculation procedure can be found in the literature [44]. For both NE and composites, the values of m and n appear to decrease and the values of k_1 and k_2 appear to increase to some extent with increasing isothermal temperatures as observed by other researchers [15,45]. Figure 7 shows plots (experimental values) of reaction rate, $\frac{d\alpha}{dt}$, versus degree of cure (α) for NE at four different isothermal temperatures along with the trends (solid lines) that would be expected from the model as per Equation 4 (using k_1, k_2, m and n) showing a good fit with the experimental data for both NE and composites. The maximum rate for both NE and composites is observed at conversion of around 10-35% for all four different isothermal temperatures, as expected for an autocatalytic reaction [46].

In the Autocatalytic Model there are two kinetic rate constants as described previously and therefore, two activation energies, E_{a1} and E_{a2}, can be obtained using the following Arrhenius

relationship for kinetic parameters k_1 and k_2

$$k(T) = A\exp(-\frac{E_a}{RT}) \qquad (7)$$

By taking logarithms of Equation 2, yields

$$\ln k = \ln A - \frac{E_a}{RT} \qquad (8)$$

Using Equation 11 the linear plots of lnk_1 versus 1/T (Figure 8) and lnk_2 versus 1/T (Figure 9) were obtained to calculate activation energies $Ea1$ and E_{a2} from the slopes of the graphs. The activation energies obtained are given in Table 3.

It can be seen that for this model as for the Kissinger and Flynn-Wall-Ozawa models, the activation energies for the curing of composites exhibited lower values compared to curing of NE (also in Table 3) supporting that the addition of fibre in epoxy enhanced the curing reaction between epoxy resin and amine curing agent. The average activation energies obtained from Kissinger and Flynn-Wall-Ozawa Models were higher than those obtained from the Autocatalytic Model. This might be due to a wide temperature range of 25-120°C used in the current study for the Autocatalytic Model. The wide temperature range might cause a decrease in the slope of the Arrhenius plot due to the large variation in the reaction constants and a consequent reduction in the activation energies.

3.1.3 Isothermal cure reactions at different epoxy resin to curing agent ratios

Table 6 summarises the time required to cure NE and composites at four different epoxy to curing agent ratios cured at 25°C. Both NE and composites had incomplete cure reactions at epoxy to curing agent ratios of 1:0.6 and 1:0.8 which is likely to be due to the deficiency in the availability of the curing agent necessary for the completion of the curing reaction. The cure reactions were complete for both NE and composites at epoxy to curing agent ratios of

1:1 and 1:1.2 and the time required for the curing was found to decrease with the increase of the curing agent as expected. It can also be seen that at the same epoxy to curing agent ratio, the time required to cure NE is longer than that for the composites which might again be caused by the enhanced nucleophilic activity of amine groups in the presence of the cellulosic fibres [40]. In this study, calculation of activation energies at different epoxy to curing agent ratios was not possible due to incomplete curing reactions at epoxy to curing agent ratios of 1:0.6 and 1:0.8 (below their stoichiometric ratio).

3.2 IFSS measurement of hemp fibre/epoxy samples

An example of the load versus displacement curve obtained in the pull-out tests on hemp fibre/epoxy samples is shown in Figure 10. From the figure, five stages can be seen [47]. During the first stage, (A to B) system slack is taken up, whilst elastic deformation of the fibre starts at point B of the second stage and continues until point C where the stress field around the embedded fibre is sufficient to initiate crack propagation. Thus, debonding (the third stage) initiates at point C and continues until point D where a sudden drop in load is observed due to the complete debonding (the fourth stage). During the fifth stage, (E to F), pull-out of the fibre occurs. All the hemp fibre-epoxy resin samples showed similar graphs with a sudden drop in the load at point D [48].

Figures 11 and 12 show the debonding force for the UTFE and ATFE samples, respectively, at four different epoxy resin to curing agent ratios cured at room temperature. Linear relationships between the debonding force and embedded length were obtained for all fibre-epoxy resin samples, though with different slopes. The higher slopes obtained for debonding force versus embedded length (at all epoxy resin to curing agent ratios) for the ATFE samples compared to the UTFE samples suggested a stronger interface between alkali treated fibre and epoxy resin. Figures 13 and 14 show the IFSS values calculated by dividing the debonding

force by the interfacial area of the UTFE and ATFE samples (Equation 5) respectively [49]. The highest IFSS value for ATFE samples was 5.2 MPa which was higher than the highest value of 2.7 for UTFE samples, supporting that there was a stronger interface between alkali treated fibre and epoxy resin. Higher interfacial bonding for ATFE samples can be explained by the increase of available –OH groups as observed by FTIR analysis [50] due to alkali treatment. These would be expected to occur due to removal of the non-cellulosic materials covering the cellulose –OH groups and also due to increased roughness, which would generally increase the surface area of the fibre. Increased exposure of cellulose –OH groups would provide increased potential for hydrogen and covalent bonding with amine (NH_2) groups of the curing agent and epoxide or -OH group of epoxy resin. In addition to increasing –OH groups for bonding, increased surface roughness would also provide for better mechanical interlocking with epoxy resin [51,52].

From the slopes of the graphs of debonding force versus embedded length (Figures 11 and 12) it can be determined that for both UTFE and ATFE samples, the best fibre/epoxy bonding is for E_1C_1 followed by $E_1C_{1.2}$ and $E_1C_{0.8}$, and finally for $E_1C_{0.6}$. It had been thought that increasing the curing agent to epoxy resin ratio above its stoichiometry might have allowed for extra active hydrogen groups to form hydrogen bonding with the –OH groups of fibre to provide increased interfacial bonding. However, the fact the E_1C_1 samples were found to have higher IFSS than $E_1C_{1.2}$ samples suggests that either matrix integrity has been compromised or reduced wettability has been a factor. The best wettability would be expected to occur for resins with the lowest viscosity for which curing time as described previously could be used to indicate the relative order; resins with the longest curing time would be expected to have the lowest viscosity. Therefore, the best wettability would be expected for $E_1C_{0.6}$ followed by $E_1C_{0.8}$ and E_1C_1, and finally for $E_1C_{1.2}$. Better wetting not increasing the fibre/epoxy bonding in $E_1C_{0.6}$ and $E_1C_{0.8}$ samples may be due to reduced matrix integrity or reduced interfacial

bonding.

IFSS was found to decrease with embedded length for both UTFE and ATFE samples, such that ATFE samples were found to be more variable than UTFE samples (Figures 13 and 14). This variation of IFSS versus embedded length indicates a brittle interface fracture behaviour as reported by other researchers [53]. A non-constant function arises with pull-out by brittle fracture due to the requirement of a critical crack length, which, once achieved, requires no further increase of stress for a longer embedded fibre length. As previously discussed, the increased access of –OH groups is likely to contribute to the increase in interfacial strength and therefore increased brittle behaviour of the ATFE samples. The degree of inconsistency for both UTFE and ATFE samples generally increased with increase in IFSS which would be expected to bring about more brittle behaviour.

3.3 Effects of epoxy to curing agent ratio on composite tensile properties

Figure 15 shows the tensile properties of 30 and 40 wt% UTFE and ATFE composites produced using four different epoxy to curing agent ratios. Higher σ and E were obtained at the higher fibre content of 40 wt% than at 30 wt%, as would be expected with successful reinforcement. It can also be seen that σ and E increased for both UTFE and ATFE composites as the epoxy resin to curing agent ratio was varied from 1:0.6 to 1:1. σ was then found to decrease, although E still increased when the epoxy to curing agent ratio was decreased further to 1:1.2.

Composites produced with alkali treated fibres were found to exhibit better tensile properties than those with untreated fibres. This could be due to the increased bonding of epoxy resin with fibres due to the increased availability of fibre –OH groups as well as surface roughening upon alkali treatment as discussed previously.

3.4 Effect of curing temperature on composite tensile properties

Figure 16 shows tensile properties of 40 wt% UTFE and ATFE composites produced at three different curing temperatures of 25, 70 and 120°C. From the results it can be seen that σ and E are higher at 70°C than at 25°C for both UTFE and ATFE composites, but decrease as the curing temperature is increased further to 120°C. σ and E are consistently higher for ATFE than for UTFE composites as seen in the previous section.

The increase in curing temperature would be expected to decrease the viscosity of the epoxy resin [54,55], which could lead to better penetration of the resin between the fibres and result in an increase in fibre/resin wetting. Increased fibre/resin wetting could result in a stronger interface which could lead to an increase in σ and E and a decrease in FS of the composites. However, composite production by rapid curing at 120°C might not allow sufficient time for epoxy resin to penetrate between the fibres as effectively as it did during composite production by curing at 70°C, and might also generate higher internal stresses which could result in decreased tensile properties as reported by Hepworth, Bruce, Vincent and Jeronimidis [56]. Figures 17(a) and 17(b) show SEM micrographs of fracture surfaces of tensile tested specimens with 40 wt% alkali treated fibres produced at 120°C and 70°C curing temperatures, respectively. It can be seen from the figures that better wetting of fibre was obtained for the composites produced with a curing temperature of 70°C.

4. Conclusions

Two dynamic models (the Kissinger and Flynn-Waal-Ozawa Models) and an isothermal model (the Autocatalytic Model) provided good fits for the experimental data obtained from isothermal differential scanning calorimetry scans of neat epoxy (NE) and 40 wt% fibre composites. The activation energies for the curing of composites exhibited lower values compared to curing of NE. This indicates that the addition of fibre in epoxy resin enhanced

the curing reaction between epoxy resin and amine curing agent which could be due to higher nucleophilic activity of the amine groups of the curing agent in the presence of fibres. The average activation energies obtained from dynamic models were higher than those obtained from the isothermal model. This might be due to the wide temperature range of 25-120°C used in this study leading to a decrease in the slope of the Arrhenius plot due to the large variation in the reaction constants.

Higher IFSS values were obtained for alkali treated fibre/epoxy samples than for untreated fibre/epoxy samples supporting that there was a stronger interface between alkali treated fibre and epoxy resin. This is believed to be due to the increased exposure of –OH groups and surface roughness upon alkali treatment of the fibres. The highest IFSS value of 5.2 MPa achieved was at an epoxy to curing agent ratio of 1:1. Higher IFSS of alkali treated fibre composites appears to have resulted in higher tensile strength, σ and Young's modulus, E, compared to untreated fibre composites. The largest increase in σ was obtained for ATFE composites with an epoxy to curing agent ratio of 1:1 and the largest increase in E was obtained with an epoxy to curing agent ratio of 1:1.2. σ and E of the composites were found to be higher at 70°C than at 25°C for both UTFE and ATFE composites, but they were found to decrease as the curing temperature was increased further to 120°C, suggesting that 70°C gave the best compromise in terms of resin viscosity and time to cure, as well as reduction of internal stresses.

5. References

1. I. K. Varma and V. B. Gupta, in: *Comprehensive Composite Materials*, A. Kelly and C. Zweben (Eds), Vol. 2, pp. 3–4. Elsevier Science Ltd., Oxford (2000).
2. P. K. Mallick, *Fiber-Reinforced Composites: Materials, Manufacturing, and Design*. Marcel Dekker, New York, NY (1993).
3. R. G. C. Arridge and J. H. Speake, *Polymer* 13, 443 (1972).

4. J. M. Charlesworth, *Polym. Engg. Sci.* 28, 221 (1988).

5. H. Stutz and J. Mertes, *J. Polym. Sci. Part A: Polym. Chem.* 31, 2031 (1993).

6. S. Hwang and G. Lee, *Eur. Polym. J.* 36, 2305–2308 (2000).

7. X. Wang and Q. Zhang, *Eur. Polym. J.* 40, 385–395 (2004).

8. Y. Liang, D. Jing, Q. Bao-jun and S. Wen-fang, *J. Chem. Res. Chinese Universities* 22, 118–122 (2006).

9. A. Catalani and M. G. Bonicelli, *Thermochimica Acta* 438, 126–129 (2005).

10. H. E. Kissinger, *Anal. Chem.* 29, 1702–1706 (1957).

11. S. Moteserrat and J. Malek, *Thermochimica Acta* 228, 47 (1993).

12. J. H. Flynn and L. A. Wall, *J. Appl. Polym. Sci., Part B* 4, 323 (1966).

13. O. A. Ozawa, *J. Thermal. Anal.* 2, 301 (1970).

14. M. R. Kamal, *Polym. Engg. Sci.* 14, 23 (1974).

15. F. Y. C. Boey and W. Qiang, *Polymer* 41, 2081–2094 (2000).

16. K. Horie, H. Hiura, M. Souvada, I. Mita and H. Kambe, *J. Appl. Polym. Sci.: Polym. Chem.* 8, 1357 (1970).

17. P. Favre and J. Perrin, *J. Mater. Sci.* 7, 1113–1118 (1972).

18. M. R. Piggott, *Composites Sci. Technol.* 57, 853–857 (1997).

19. L. J. Broutman, in: *Interfaces in Composites*; ASTM STP 452, American Society for Testing and Materials, p. 27. Philadelphia, PA (1969).

20. A. Kelly and W. R. Tyson, *J. Mech. Phys. Solids* 12, 329 (1965).

21. L. T. Drzal, P. J. Herrera-Franco and H. Ho, in: *Comprehensive Composite Materials*, A. Kelly and C. Zweben (Eds), Vol. 5, p. 4. Elsevier Science Ltd., Oxford (2000).

22. C. Wang, *J. Mater. Sci.* 32, 483–490 (1997).

23. E. Mader, *Composites Sci. Technol.* 57, 1077–1088 (1997).

24. E. Pisanova, S. Zhandarov, E. Mader, I. Ahmad and R. J. Young, *Composites: Part A* 32, 435–443 (2001).

25. P. J. Herrera-Franco and A. Valadez-Gonzalez, *Composites: Part B* 36, 597–608 (2005).

26. A. Arbelaiz, G. Cantero, B. Fernandez, I. Mondragon, P. Ganan and J. M. Kenny, *Polym. Composites* 26, 324–332 (2005).

27. K. Lawrence, K. Wang and M. H. S. Wang (Eds), *Handbook of Industrial Waste Treatment*, Vol. 1, p. 475. Marcel Dekker, New York, NY (1992).

28. D. Robson, J. Hague, G. Newman, G. Jeronomidis and M. Ansell, *Survey of Natural Materials for Use in Structural Composites as Reinforcement and Matrices*. Woodland

Publishing Ltd., Abingdon, UK (1996).

29. D. N. Saheb and J. P. Jog, *Adv. Polym. Technol.* 18, 351–363 (1999).

30. D. G. Hepworth, D. M. Bruce, J. F. V. Vincent and G. Jeronimidis, *J. Mater. Sci.* 35, 293–298 (2000).

31. D. Ray, B. K. Sarkar, R. K. Basak and A. K. Rana, *J. Appl. Polym. Sci.* 94, 123–129 (2004).

32. A. K. Bledzki, H. P. Fink and K. Specht, *J. Appl. Polym. Sci.* 93, 2150–2156 (2004).

33. H. M. Wang and R. Postle, *Textile Res. J.* 73, 664–669 (2003).

34. J. Gassan and A. K. Bledzki, *J. Appl. Polym. Sci.* 71, 623–629 (1999).

35. R. M. Rowell, in: *Proc. Int. Conf. on Science and Technology of Composite Materials (COMAT 2001)*, Mar del Plata, Argentina, December 10–12 (2001).

36. A. K. Patrikis, M. C. Andrews and R. J. Young, *Composites Sci. Technol.* 52, 387–396 (1994).

37. M. Naffakh, M. Dumon, J. Dupuy and J. F. Gerard, *J. Appl. Polym. Sci.* 96, 660 (2005).

38. R. J. Varley, J. H. Hodgkin, D. J. Hawthorne, G. P. Simon and D. McCulloch, *Polymer* 41, 3425 (2000).

39. J. Lopez, I. Lopez-Bueno, P. Nogueira, C. Ramirez, M. J. Abad, L. Barral and J. Cano, *Polymer* 42, 1669–1677 (2001).

40. M. Ghaemy, M. Barghamadi and H. Behmadi, *J. Appl. Polym. Sci.* 94, 1049–1056 (2004).

41. L. Barral, J. Cano, J. Lopez, I. Lopez-Bueno, P. Nogueira, M. J. Abad and C. Ramirez, *J. Polym. Sci.: Part B: Polym. Phys.* 38, 351–361 (2000).

42. J. M. Salla and X. Ramis, *Polym. Engg. Sci.* 36, 835 (1996).

43. J. Mijovic, J. Kim and J. Slaby, *J. Appl. Polym. Sci.* 29, 1449 (1984).

44. J. M. Kenny, *J. Appl. Polym. Sci.* 51, 761 (1994).

45. B. Francis, V. L. Rao, G. V. Poel, F. Posada, G. Groeninckx, R. Ramaswamy and S. Thomas, *Polymer* 47, 5411–5419 (2006).

46. M. R. Kamal and S. Sourour, *Polym. Engg. Sci.* 13, 59–64 (1973).

47. K. Tanaka, K. Minoshima, W. Grela and K. Komai, *Composites Sci. Technol.* 62, 2169–2177 (2002).

48. A. Valadez-Gonzalez, J. M. Cervantes-Uc, R. Olayo and P. J. Herrera-Franco, *Composites: Part B* 30, 309–320 (1999).

49. A. Kelly, *Strong Solids*. Clarendon Press, Oxford (1973).

50. M. S. Islam, K. L. Pickering, G. W. Beckermann and N. J. Foreman, in: *Proc. Int. Conf. on Mechanical Engineering 2005 (ICME2005)*, Dhaka, Bangladesh, pp. AM–17 (2005).

51. F. L. Matthews and R. D. Rawlings, *Composite Materials: Engineering and Science*. Chapman & Hall, London (1994).

52. K. Joseph, S. Varghese, G. Kalaprasad, S. Thomas, L. Prasannakumari, P. Koshy and C. Pavithran, *Eur. Polym. J.* 32, 1243–1250 (1996).

53. A. Stamboulis, C. Baillie and E. Schulz, *Angew. Makromolekulare Chemie* 272, 117–120 (1999).

54. A. Maffezzoli, E. Calo, S. Zurlo, G. Mele, A. Tarzia and C. Stifani, *Composites Sci. Technol.* 64, 839–845 (2004).

55. A. Maffezzoli, E. Calo, S. Zurlo, G. Mele, A. Tarzia and C. Stifani, *Composites Sci. Technol.* 64, 839–845 (2004).

56. D. G. Hepworth, D. M. Bruce, J. F. V. Vincent and G. Jeronimidis, *J. Mater. Sci.* 35, 293–298 (2000).

Figure number and Caption to the figures:

Figure 1 Test specimen for single fibre pull-out tests.

Figure 2 Single fibre embedded in epoxy resin.

Figure 3 Heat flow measured by DSC during cure of NE at five different heating rates (Heat flow normalized with respect to specimen weight to show relative peak sizes).

Figure 4 Heat flow measured by DSC during cure of composites at five different heating rates (Heat flow normalised with respect to specimen weight to show relative peak sizes).

Figure 5 Plots to determine activation energies by the Kissinger model for NE and composites.

Figure 6 Plots to determine activation energies by the Flynn-Wall-Ozawa method for NE and composites.

Figure 7 Conversion rate versus degree of cure graphs for NE at four different isothermal temperatures. The solid lines show the trend expected from the Autocatalytic Model (Equation 4).

Figure 8 Arrhenius plot for the reaction constant k_1.

Figure 9 Arrhenius plot for the reaction constant k_2.

Figure 10 Typical load versus displacement curve for pull-out tests on hemp/epoxy samples.

Figure 11 Debonding force versus embedded length plots for UTFE samples at various epoxy resin to curing agent ratios.

Figure 12 Debonding force versus embedded length plots for ATFE samples at various epoxy resin to curing agent ratios.

Figure 13 IFSS values for UTFE samples found at eight different embedded lengths and four different epoxy resin to curing agent ratios. (The curved lines indicate principal trends of data points and do not represent any data fitting).

Figure 14 IFSS values for ATFE samples found at eight different embedded lengths and four different epoxy resin to curing agent ratios. (The curved lines indicate principal trends of data points and do not represent any data fitting).

Figure 15 Tensile properties of 30 and 40 wt% UTFE and ATFE composites produced at four different epoxy to curing agent ratios. Each error bar corresponds to one standard deviation.

Figure 16 Tensile properties of 40 wt% UTFE and ATFE composites produced at three different curing temperatures. Each error bar corresponds to one standard deviation.

Figure 17 SEM micrographs of fracture surfaces of tensile tested specimens with 40 wt% alkali treated fibres produced at (a) 120°C and (b) 70°C curing temperatures.

Table 1 Duration of pressure applied at each curing temperature.

Curing Temperature (^{o}C)	Duration of Pressure
25	12 hours
70	20 minutes
120	5 minutes

Table 2 Heat of reaction for NE and composites at five different heating rates.

Heating Rate, q (^{o}Cmin^{-1})	ΔH_0 (J/g)		Peak Temperature, T_m (^{o}K)	
	NE	Composites	NE	Composites
2.5	292.5	120.8	352.6	341.2
5	298.0	124.8	365.5	346.2
10	301.8	126.8	373.4	354.7
15	304.7	128.3	379.1	363.4
20	305.0	133.6	387.6	374.3
Average, ΔH_{tot}	300.4	126.86		

Table 3 Comparison of activation energies obtained by different models.

Sample	Kissinger Model	Flynn-Wall-Ozawa Model	Autocatalytic Model	
	E_a (kJ/mol)	E_a (kJ/mol)	E_{a1} (kJ/mol)	E_{a2} (kJ/mol)
NE	56.7	58.5	37.2	45.3
Composites	50.9	54.6	36.8	38.3

Table 4 Curing time, ΔH_t, and α_f for NE and composites at four different curing temperatures.

Curing Temperature (°C)	Samples	Curing Time (min)	ΔH_t (J/g)	α_f
25	NE	827	140.9	0.47
	Composites	719	65.3	0.51
50	NE	300	172.0	0.57
	Composites	191	77.9	0.61
70	NE	38	229.9	0.77
	Composites	19.5	104.3	0.82
120	NE	6.5	258.7	0.86
	Composites	4.5	114.4	0.90

Table 5 Autocatalytic model parameters for NE and composites.

Sample	Curing Temperature (^{o}C)	m	n	$k_1 \times 10^3$ (min^{-1})	$k_2 \times 10^3$ (min^{-1})
NE	25	0.83	4.64	3.79	9.1
	50	0.68	3.72	17.91	100.2
	70	0.39	2.52	38.12	291.4
	120	0.35	1.75	126.97	715.7
Composites	25	1.18	3.98	6.30	19.2
	50	0.81	3.27	24.93	159.6
	70	0.67	1.67	43.33	436.2
	120	0.29	0.51	202.35	775.2

Table 6 Curing time of NE and composites at four different epoxy to curing agent ratios cured at 25°C.

Epoxy to Curing Agent Ratio	Samples	Curing Time (min)
1:0.6	NE	Incomplete Curing After 1440 min
	Composites	Incomplete Curing After 1440 min
1:0.8	NE	Incomplete Curing After 1440 min
	Composites	Incomplete Curing After 1440 min
1:1	NE	827
	Composite	719
1:1.2	NE	641
	Composite	528
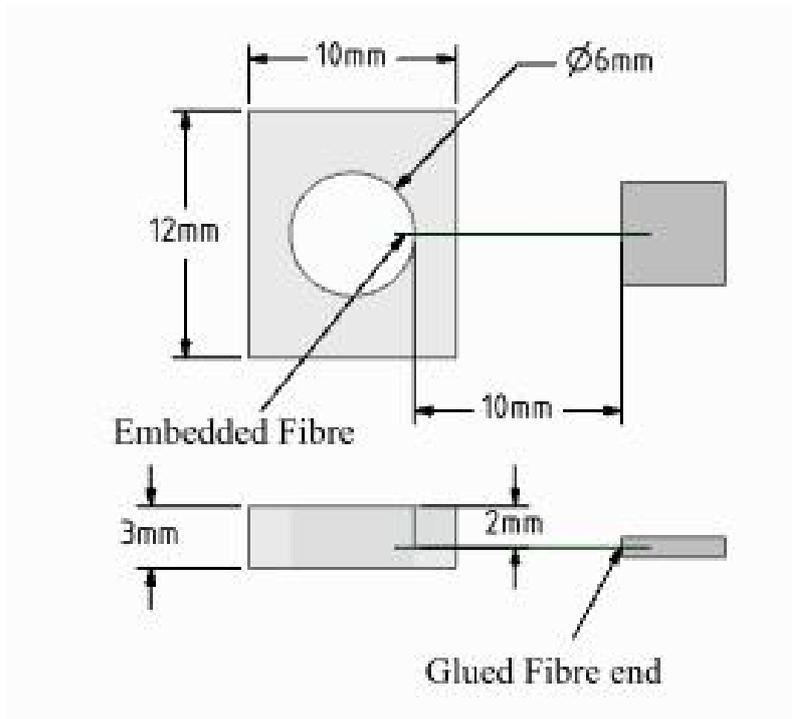
Figure 1
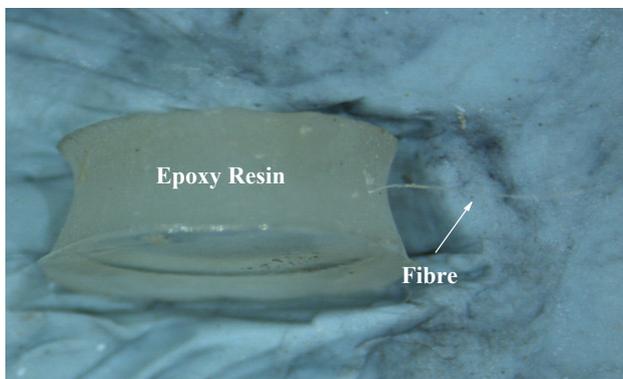
Figure 2
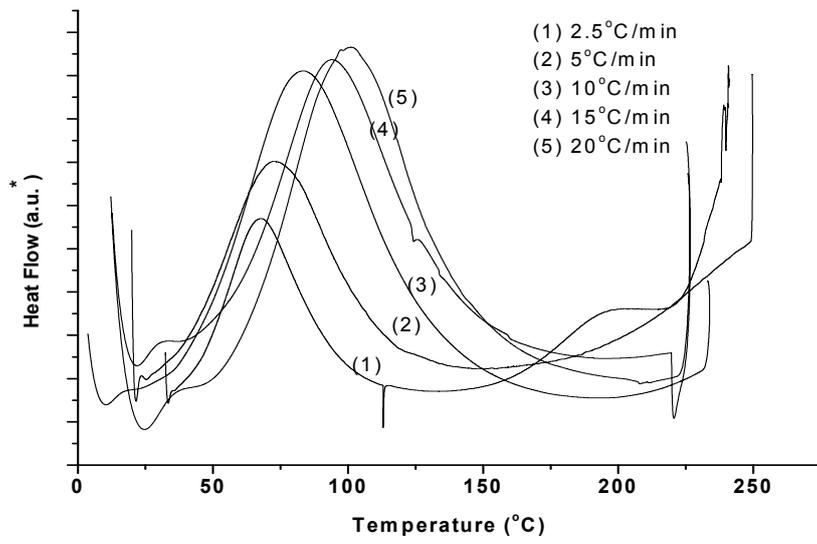
Figure 3
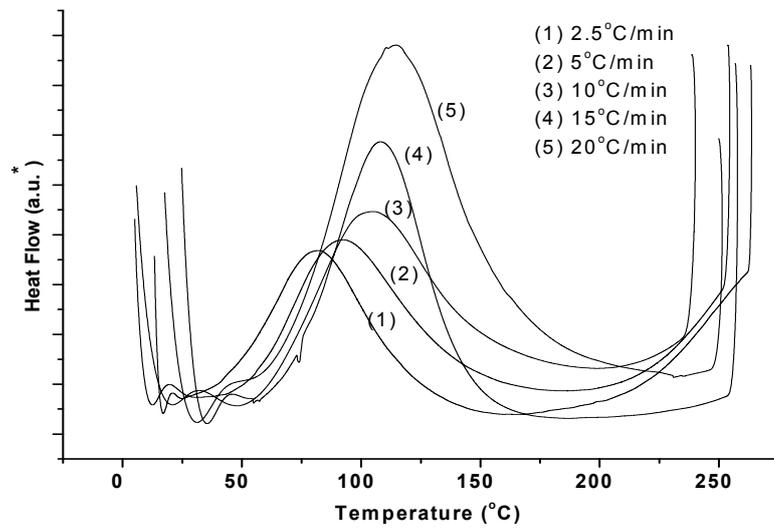
Figure 4
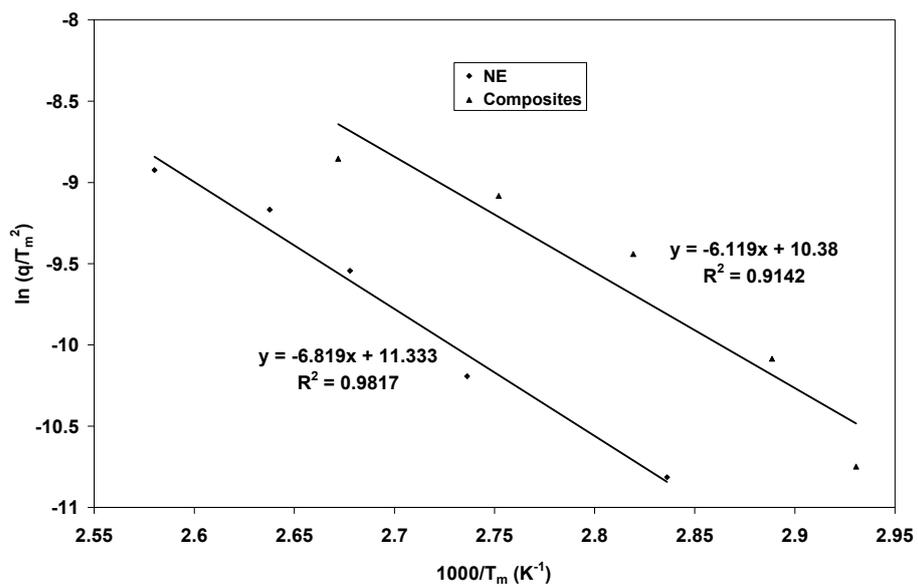
Figure 5
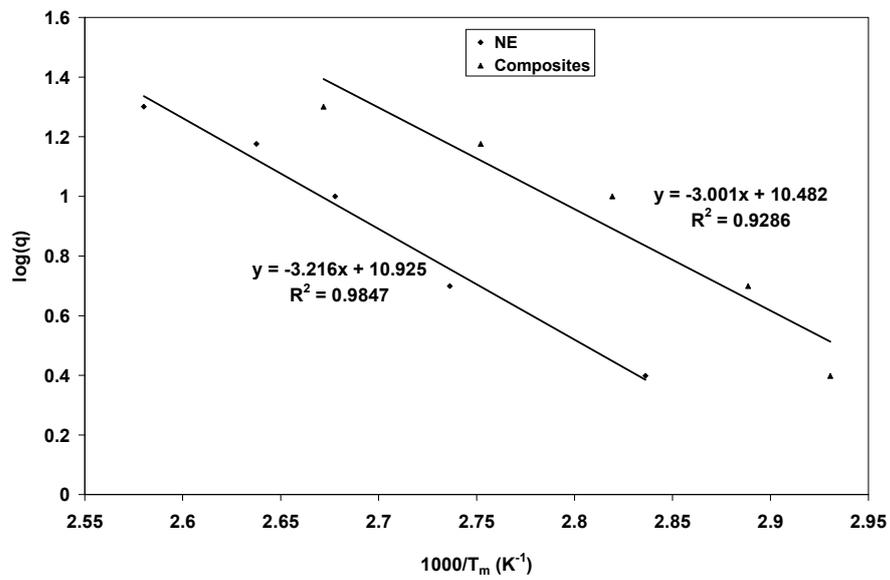
Figure 6
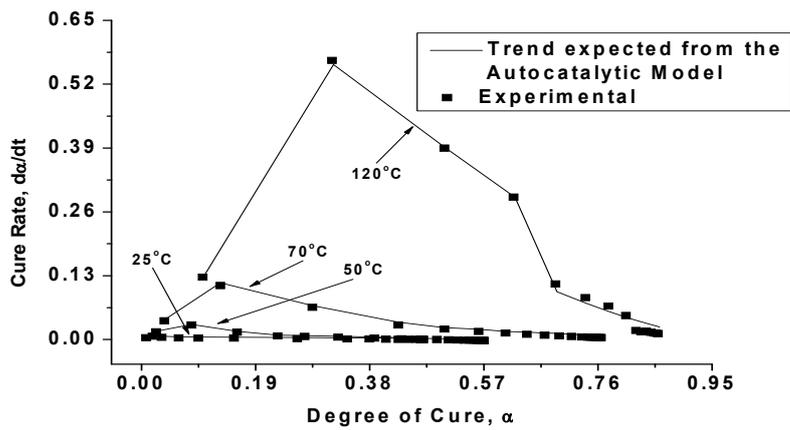
Figure 7
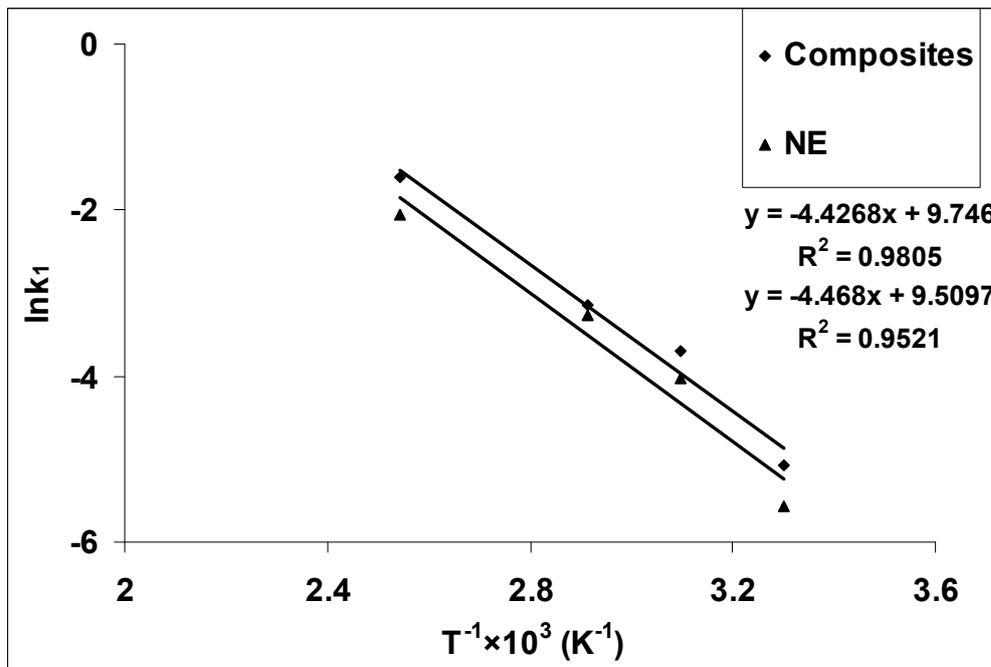
Figure 8
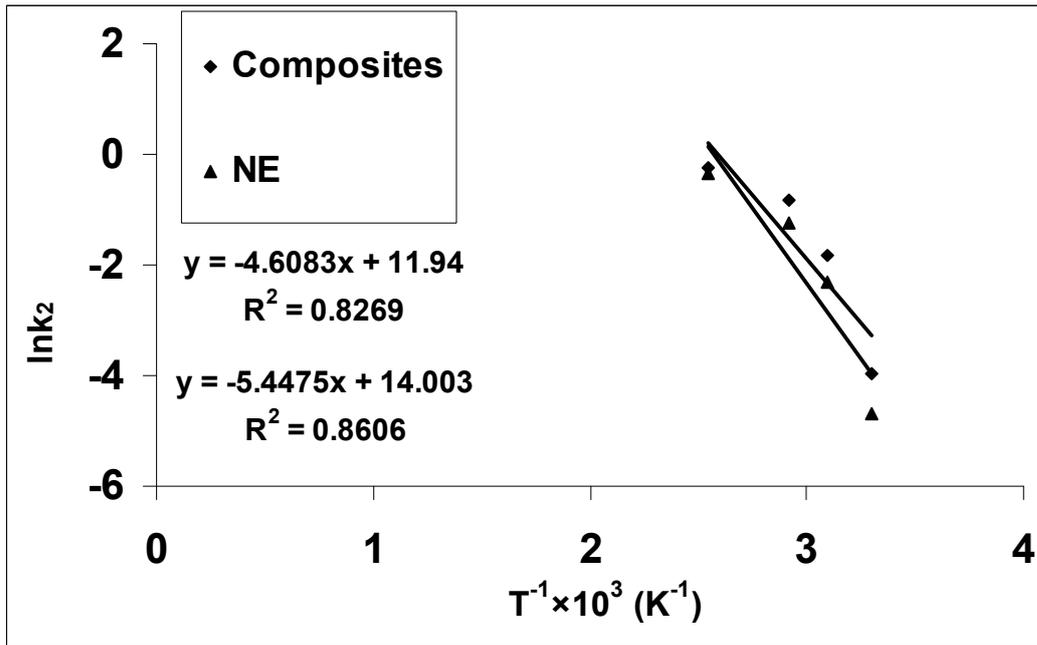
Figure 9
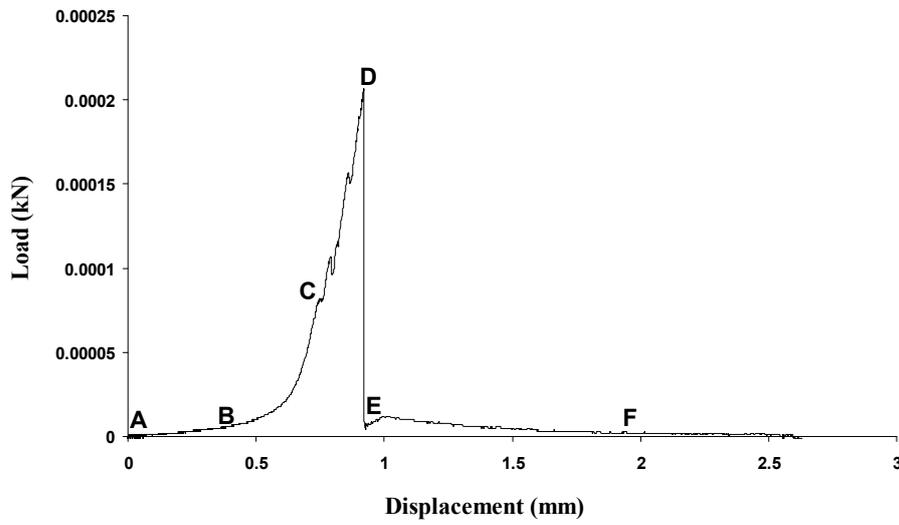
Figure 10
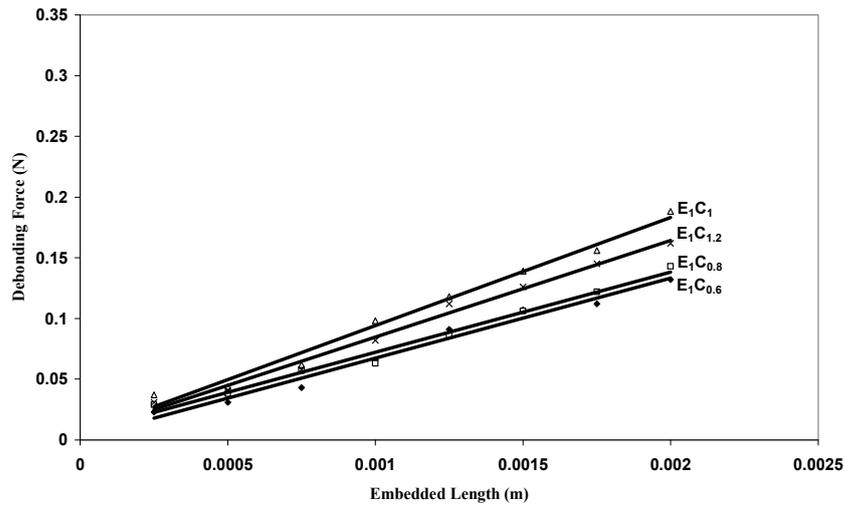
Figure 11
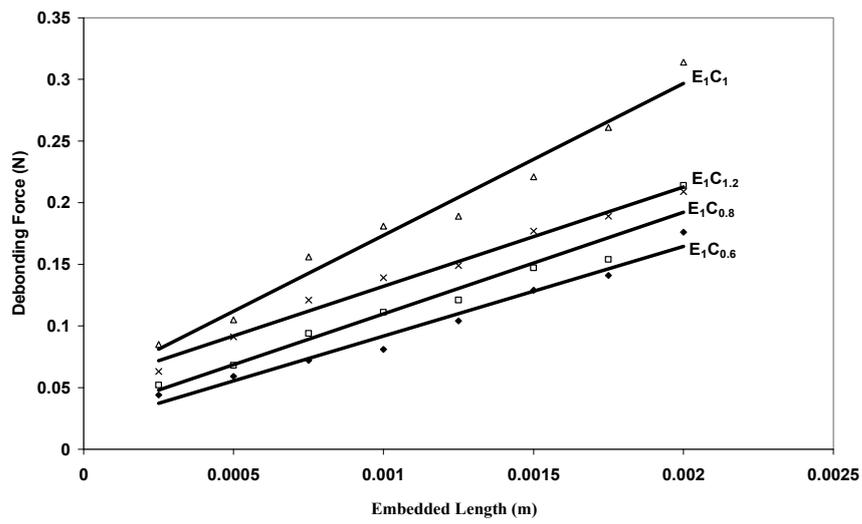
Figure 12
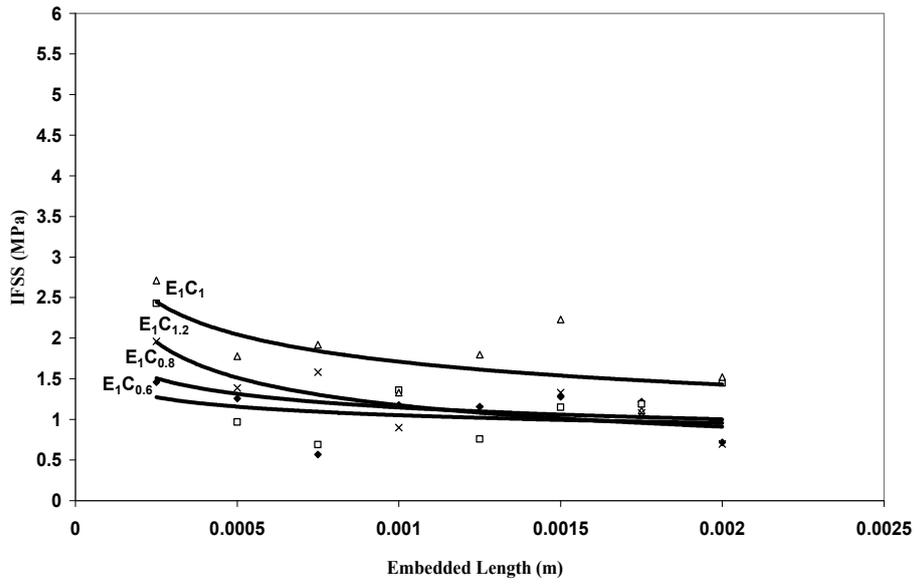
Figure 13
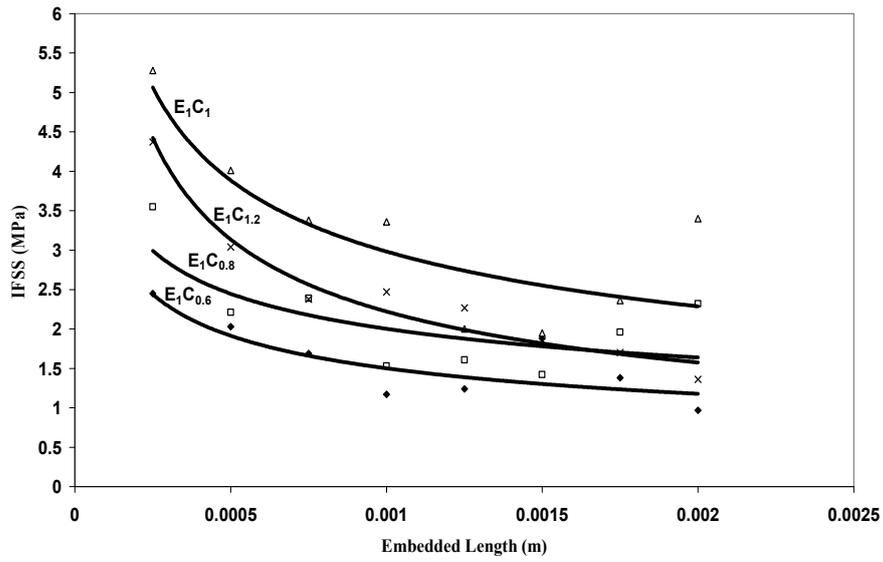
Figure 14

Figure 15

Figure 16

Poor
Fibre
Wetting

Good Fibre
Wetting

(a)   (b)

Figure 17